Available online at www.sciencedirect.com
SCIENCE DIRECT®
Geochimica et Cosmochimica Acta 70 (2006) 446–460
Geochimica
www.elsevier.com/locate/gca

Experimental investigation of single carbon compounds under hydrothermal conditions

Jeffrey S. Seewald [a,*], Mikhail Yu. Zolotov [b], Thomas McCollom [c]

[a] Department of Marine Chemistry and Geochemistry, Woods Hole Oceanographic Institution, MS #4, Woods Hole, MA 02543, USA
[b] Department of Geological Sciences, Arizona State University, Tempe, AZ 85287-1404, USA
[c] Center for Astrobiology and Laboratory for Atmospheric and Space Physics, University of Colorado, Boulder, CO 80309, USA

Received 31 January 2005; accepted in revised form 8 September 2005

Abstract

The speciation of carbon in subseafloor hydrothermal systems has direct implications for the maintenance of life in present-day vent ecosystems and possibly the origin of life on early Earth. Carbon monoxide is of particular interest because it represents a key reactant during the abiotic synthesis of reduced carbon compounds via Fischer–Tropsch-type processes. Laboratory experiments were conducted to constrain reactions that regulate the speciation of aqueous single carbon species under hydrothermal conditions and determine kinetic parameters for the oxidation of CO according to the water water–gas shift reaction ($CO_2 + H_2 = CO + H_2O$). Aqueous fluids containing added CO_2, CO, HCOOH, $NaHCO_3$, NaHCOO, and H_2 were heated at 150, 200, and 300 °C and 350 bar in flexible-cell hydrothermal apparatus, and the abundances of carbon compounds was monitored as a function of time. Variations in fluid chemistry suggest that the reduction of CO_2 to CH_3OH under aqueous conditions occurs via a stepwise process that involves the formation of HCOOH, CO, and possibly CH_2O, as reaction intermediaries. Kinetic barriers that inhibit the reduction of CH_3OH to CH_4 allow the accumulation of reaction intermediaries in solution at high concentrations regulated by metastable thermodynamic equilibrium. Reaction of CO_2 to CO involves a two-step process in which CO_2 initially undergoes a reduction step to HCOOH which subsequently dehydrates to form CO. Both reactions proceed readily in either direction. A preexponential factor of 1.35×10^6 s^{-1} and an activation energy of 102 kJ/mol were retrieved from the experimental results for the oxidation of CO to CO_2. Reaction rates amongst single carbon compounds during the experiments suggest that ΣCO_2 ($CO_2 + HCO_3^- + CO_3^{2-}$), CO, $\Sigma HCOOH$ ($HCOOH + HCOO^-$), and CH_3OH may reach states of redox-dependent metastable thermodynamic equilibrium in subseafloor and other hydrothermal systems. The abundance of CO under equilibrium conditions is strongly dependent on temperature, the total carbon content of the fluid, and host-rock lithology. If crustal residence times following the mixing of high-temperature hydrothermal fluids with cool seawater are sufficiently long, reequilibration of aqueous carbon can result in the generation of additional reduced carbon species such as HCOOH and CH_3OH, and the consumption of H_2. The present study suggests that abiotic reactions involving aqueous carbon compounds in hydrothermal systems are sufficiently rapid to influence metabolic pathways utilized by organisms that inhabit vent environments.

1. Introduction

In recent years, abiotic chemical reactions have been discussed as a potential mechanism for the formation of reduced carbon compounds in seafloor hydrothermal systems, where CO_2, CO, CH_4, and C_{2+} hydrocarbons are present as major and trace components. Because the substantial fluid flux through deep-sea hot-springs represents a potentially significant source of carbon and energy to support microbial activities in surface and sub-surface habitats, the possibility that abiotic processes may influence the speciation of carbon in vent fluids has direct implications for the maintenance of life in present-day hydrothermal environments. Furthermore, models developed to account for the origin of life within a hydrothermal setting on the early Earth typically invoke abiotic chemical

* Corresponding author. Fax: +1 508 457 2164.
E-mail address: jseewald@whoi.edu (J.S. Seewald).

0016-7037/$ - see front matter © 2005 Elsevier Inc. All rights reserved.
doi:10.1016/j.gca.2005.09.002

processes as being responsible for the production of precursor organic compounds from which life formed and evolved. Despite the significant role that aqueous carbon compounds play in a broad spectrum of geochemical and biological processes, reactions that regulate the abundance of aqueous carbon compounds at elevated temperatures and pressures are poorly constrained.

Abiotic synthesis of organic compounds in hydrothermal environments is commonly attributed to Fischer–Tropsch-type processes that involve the reduction of CO_2 and/or CO by H_2 on a catalytic surface to form bound methylene groups that polymerize into long chain hydrocarbons (Anderson, 1984). Although the process can proceed with CO_2 and H_2 as initial reactants, rates and yields are substantially enhanced by the presence of CO. It is generally believed that formation of hydrocarbons from CO_2 involves an initial reduction step to form CO by the water–gas shift reaction as follows:

$$CO_2 + H_2 = CO + H_2O. \quad (1)$$

Because this reaction allows CO_2 to be used as feedstock for hydrocarbon formation by Fischer–Tropsch synthesis, it has been the focus of much attention in the engineering literature. The overall process represented by reaction (1) is a two-step process involving the formation of a formic acid intermediary that subsequently decomposes to CO according to the reactions:

$$CO_2 + H_2 = HCOOH \quad (2)$$

$$HCOOH = CO + H_2O. \quad (3)$$

(Elliott and Sealock, 1983; Melius et al., 1991; Rice et al., 1998). At temperatures below ~800 °C, the water–gas shift reaction is exceedingly slow when occurring in a gas phase at low water fugacities and does not occur on a laboratory time scale unless a catalyst is present (Burkhard and Ulmer, 1995; Deines et al., 1974; Huebner, 1987; Nafziger et al., 1971; Ulmer, 1984). The rates increase substantially at higher water fugacities under supercritical conditions (Rice et al., 1998). At sub- and near critical temperatures typical for seafloor hydrothermal systems, the rates of reaction (1) are poorly known.

In addition to the water–gas shift reaction, there are many other processes that may influence the speciation of carbon under hydrothermal conditions. Reactions between single carbon compounds in the C–H–O system are limited to formation of CO_2, CO, formic acid (HCOOH), formaldehyde (CH_2O), methanol (CH_3OH), and CH_4 which can be generalized by the sequence in Fig. 1. If formation of carbon–carbon bonds is considered, an almost limitless number of reactions are possible that may influence carbon speciation. It is important to recognize that although Fischer–Tropsch-type processes may produce CH_4 and longer chain hydrocarbons from CO_2, it should not be viewed as the only mechanism available to produce reduced carbon species at elevated temperatures and pressure. In particular, production of CH_4 may occur in

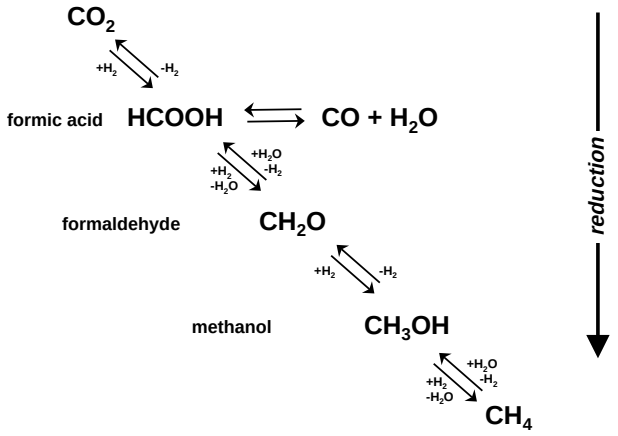

Fig. 1. Schematic representation of redox reactions that may regulate the speciation of single carbon compounds under hydrothermal conditions.

aqueous solution without the involvement of a heterogeneous catalyst or gas phase. This study was conducted to investigate aqueous processes that influence the speciation of single carbon compounds under conditions typical of seafloor hydrothermal systems and builds on previous work that shows formic acid and CO_2 equilibrate rapidly at the prevailing redox conditions in many low-temperature hydrothermal environments (McCollom and Seewald, 2003). In particular, an experiment was designed to constrain the rates of reactions that regulate the abundance of CO as a function of pH, redox conditions, and temperature in the absence of an added catalyst. The results have direct applications to models that account for abiotic synthesis and the speciation of carbon in hydrothermal systems on Earth and other solar system bodies.

2. Methods

Flexible-cell hydrothermal apparatus (Seyfried et al., 1987) was used for the experiment. This equipment consists of a flexible gold reaction cell with a titanium closure piece and exit tube that is encased in a stainless-steel pressure vessel. External control of pressure within the steel vessel allows elimination of a vapor head-space within the flexible reaction cell. A stainless-steel valve attached to the exit tube allows removal of fluid from the reaction cell for chemical analysis without disturbing the temperature and pressure conditions of an experiment. The composition of reactants within the reaction cell can be modified by injecting fluids through the sampling valve using a high pressure pump. The experiment was conducted at 150, 200, and 300 °C and 350 bar. Prior to the experiment, titanium components of the reaction cell were heated at 400 °C in air to form a chemically inert TiO_2 surface layer. Because the goal of this investigation was to examine the uncatalyzed rates of aqueous reactions involving single carbon compounds, heterogeneous catalysts were not added during any phase of the experiment. Although the possibility exists that some of the reactions being studied may be catalyzed

by the gold–titanium reaction cell, previous studies have not revealed catalytic properties for Au and TiO_2 with respect to carbon chemistry under hydrothermal conditions (Bell and Palmer, 1994; Bell et al., 1994; McCollom and Seewald, 2001, 2003).

The general approach used to examine equilibration of CO and CO_2 during this study involved creating thermodynamic disequilibrium within the chemical system and subsequently monitoring changes in fluid chemistry as a function of time. At chemical equilibrium according to reaction (1), fluid composition is constrained by the mass action expression:

$$K_{eq} = \frac{a_{CO} a_{H_2O}}{a_{CO_2} a_{H_2}}, \quad (4)$$

where K_{eq} is the equilibrium constant and a_j is the activity of aqueous species j. Chemical disequilibrium was induced by a variety of methods including addition of CO_2, H_2, or CO, varying pH, and dilution of reaction cell contents with deionized water (Table 1). In the latter case, equal magnitude reductions in the aqueous concentrations of all dissolved gases in the reaction cell by dilution induce disequilibria because the denominator in Eq. (4) is affected to a greater extent than the numerator. Varying temperature was less effective as a means to induce disequilibria during this study because the equilibrium constant for reaction (1) does not change substantially in the temperature range of 150–300 °C (Fig. 2).

Owing to technical difficulties associated with injecting large amounts of gaseous reactants into the reaction cell,

Table 1
Concentrations of selected aqueous species during heating at 150–300 °C and 350 bar

Time (h)	Temp (°C)	H_2 (mmol/kg)	ΣCO_2 (mmol/kg)	CO (mmol/kg)	Na (mmol/kg)	CH_4 (mmol/kg)	CH_3OH (mmol/kg)	ΣHCOOH (mmol/kg)
0.0	300	0	0	0	na	0	0	175
48.0	300	171	163	0.83	na	0.0060	0.37	0.38
216.0	300	176	165	0.79	na	0.012	0.97	0.37
266.0	200	Temperature reduced to 200 °C						
290.0	200	167	164	0.73	na	0.016	1.1	3.1
381.2	200	na	na	na	na	na	1.2	4.1
385.0	200	Added 28.8 g H_2O to 14.3 g H_2O in reaction cell						
385.0[a]	200	55	54	0.24	na	0.0054	0.41	1.36
409.3	200	59	56	0.097	na	0.0087	0.39	0.68
502.8	200	59	54	0.078	na	0.0089	0.38	0.54
509.8	150	Temperature reduced to 150 °C						
551.5	150	na	50	0.066	na	0.0073	0.37	0.67
572.7	150	57	na	0.071	na	na	na	0.73
721.5	150	Added CO and 29.7 g H_2O to 13.5 g H_2O in reaction cell						
721.5[a]	150	18	16	⩾172	na	0.0023	0.12	0.23
736.6	150	na	15	172	na	0.0044	na	0.98
766.1	150	16	16	172	na	0.0045	0.10	1.1
814.1	150	17	20	176	na	0.0044	0.10	3.3
839.6	150	24	na	158	na	na	na	4.1
861.0	150	25	22	143	na	0.0043	0.11	4.7
862.8	200	Increased temperature to 200 °C						
868.8	200	42	40	133	na	0.0045	0.10	8.6
870.8	200	50	na	126	na	na	na	9.7
885.5	200	89	82	86	na	na	0.11	14
894.0	200	na	na	73	na	na	na	na
918.0	200	146	na	31	na	na	na	12
1174.5	200	na	173	1.0	na	0.14	1.7	4.4
1200.3	200	166	na	na	na	na	2.0	4.5
1247.8	199	Added 34.6 g of 172 mmol/kg $NaH^{13}CO_3$ to 2.6 g H_2O in reaction cell						
1247.8[a]	199	12	172	0.072	160	0.010	0.15	0.32
1314.8	199	6.5	152	na	162	0.011	0.16	3.1
1509.7	199	2.4	152	0.00028	163	0.012	0.15	7.0
1674.3	199	1.4	151	0.00040	160	0.011	0.16	7.7
1679.7	300	Increased temperature to 300 °C						
1867.2	300	19	138	0.0059	161	0.020	0.030	21
1868.2	300	Added 35.9 g of 195 mmol/kg NaHCOO to 8.0 g H_2O in reaction cell						
1868.2[a]	300	4.2	28	0.0011	189	0.0037	0.006	163
1870.5	298	65	89	0.023	192	0.0044	0.002	93
1872.6	299	77	103	0.021	192	0.0044	0.003	80
2228.8	299	93	102	0.018	195	0.011	0.21	81

na, not analyzed.

[a] Concentrations immediately after injection are calculated from the amount and composition of fluids injected and preexisting in the reaction cell at the time of injection.

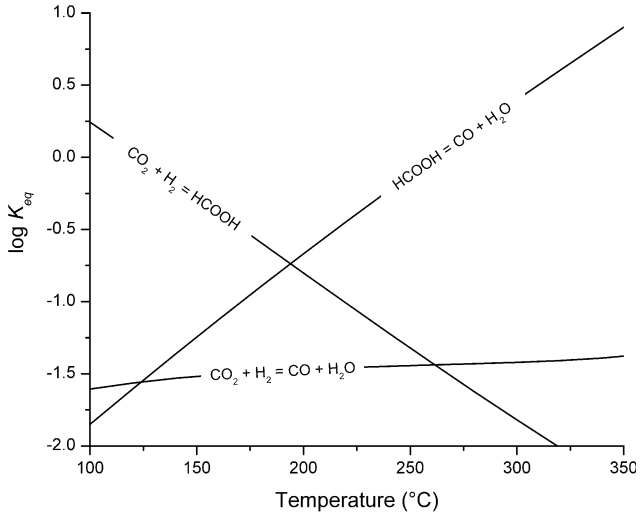

Fig. 2. Temperature dependence of the equilibrium constant (K_{eq}) at 350 bar for selected aqueous reactions involving single carbon compounds. Requisite thermodynamic data for the construction of this figure are from the compilation of Johnson et al. (1992) and Shock (1995).

addition of initial excess CO_2 and H_2 was achieved by injecting formic acid, which rapidly decomposes to CO_2 and H_2 at the conditions of the experiment (McCollom and Seewald, 2003). Isotopically labeled formic acid (99% $H^{13}COOH$, Cambridge Isotope Labs) was used for this purpose to allow unequivocal identification of carbon sources and sinks during the experiment. Addition of unlabeled CO involved initially dissolving the gas in deionized water in a length of high pressure tubing before injection into the reaction cell. The activity of H^+ was varied by injecting either sodium bicarbonate ($NaHCO_3$) or sodium formate (NaHCOO) solutions. Isotopically labeled sodium bicarbonate was used for this purpose (99% $NaH^{13}CO_3$, Cambridge Isotope Labs) after 1248 h to replenish the inventory of ^{13}C present in solution.

Throughout the course of the experiment, several fluid aliquots were removed from the reaction cell into glass gas-tight syringes on a given sampling occasion and analyzed for the concentration of dissolved species. Total dissolved CO_2 ($\Sigma CO_2 = CO_2 + HCO_3^- + CO_3^{2-}$) and C_1–C_6 hydrocarbons were analyzed using a purge and trap apparatus interfaced directly to a gas chromatograph equipped with serially connected thermal conductivity and flame ionization detectors and a Porapak-Q packed column. Complete extraction of all carbonate species as CO_2 was ensured by the presence of 25 wt% phosphoric acid in the purge cell. Dissolved CO and H_2 were analyzed following a headspace extraction by gas chromatography using a thermal conductivity detector and 5 Å molecular sieve packed column. Total dissolved formate ($\Sigma HCOOH = HCOOH + HCOO^-$) and Na^+ were determined by ion chromatography with conductivity detection. Methanol and formaldehyde were determined by split injection of aqueous samples into a gas chromatograph equipped with an EC-WAX column and a flame ionization detector. Selected fluid samples were analyzed on a benchtop mass spectrometer (Hewlett Packard 5973 mass selective detector) to determine whether ^{13}C was being incorporated into methanol and CH_4. Analytical uncertainties for all chemical species measured during this study are estimated at $\pm 5\%$ (2σ).

Concentrations of dissolved species in the reaction cell immediately after fluid addition were calculated from the amount and composition of fluids injected and known to exist in the reaction cell at the time of injection. Due to technical limitations associated with the addition of gaseous CO, it was not possible to accurately determine the amount injected. Accordingly, the initial concentration of CO immediately after injection at 721.5 h is assumed to be equal to or greater than the concentration measured at 736.6 h (Table 1). This assumption has no impact on our interpretation of the experimental results since the calculated fluid composition at 721.5 h was not used for kinetic or thermodynamic assessments (see below).

The extent of chemical equilibrium during each stage of the experiment was evaluated by comparing measured concentrations of dissolved species with values predicted for equilibration of the reactions of interest. Requisite thermodynamic data for these calculations were generated from the SUPCRT92 database (Johnson et al., 1992) and additional data from Shock (1995). In situ pH values were calculated using the computer program EQ3NR which takes into account the formation of aqueous complexes, activity coefficients of aqueous species, and carbon speciation (Wolery, 1992). In situ pH could not be calculated from measured pH (25 °C) due to extensive exsolution of aqueous CO_2 upon removal of fluid samples from the high pressure reaction cell into gas-tight syringes at ambient conditions.

3. Results

3.1. CO–CO_2 equilibration

The initial phase of the experiment involved heating a 175 mmol/kg formic acid solution at 300 °C. Rapid decomposition of the formic acid resulted in almost complete conversion to equimolar concentrations of H_2 and CO_2 within the first 48 h of reaction, after which concentrations remained constant (Table 1, Fig. 3A). Production of aqueous CO was observed in the early stages of reaction, reaching concentrations of 0.83 mmol/kg in the first sample, and then remained constant with time. The concentration of ΣHCOOH decreased to 0.38 mmol/kg during the initial 48 h of reaction and also remained constant with time. The measured steady state abundances of H_2, ΣCO_2, CO, and ΣHCOOH are consistent with values predicted for thermodynamic equilibrium according to reactions (1)–(3) (Fig. 3A). At the relatively low in situ pH ($\leqslant 3$) of this experiment, $HCOOH_{(aq)}$ and $CO_{2(aq)}$ are the predominant species for ΣHCOOH and ΣCO_2, respectively (Fig. 4). The similarity of observed and equilibrium fluid compositions in conjunction with steady state concentrations of H_2, ΣCO_2, CO, and ΣHCOOH strongly suggests that the

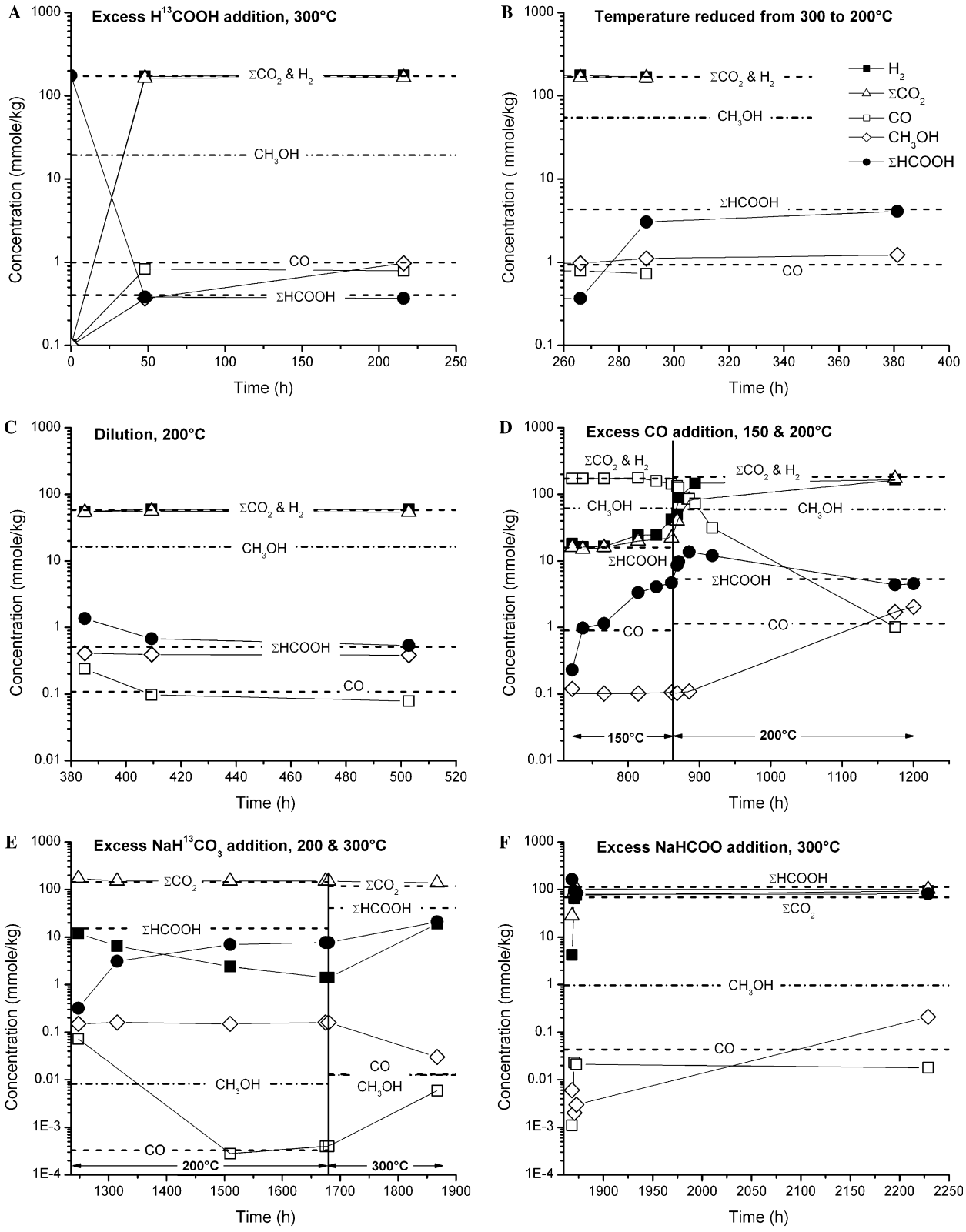

Fig. 3. Variations in the concentrations of dissolved species during reaction of aqueous solutions at (A) 300 °C following addition of $H^{13}COOH$, (B) 200 °C following reduction in temperature from 300 °C, (C) 200 °C following dilution with deionized H_2O, (D) 150 and 200 °C following addition of CO, (E) 200 and 300 °C following addition of $NaH^{13}CO_3$, and (F) 300 °C following addition of NaHCOO. The dashed horizontal lines represent predicted concentrations of the indicated species at thermodynamic equilibrium assuming kinetic barriers prevent significant quantities of CH_4 and CH_3OH from forming. In figures (E and F), the equilibrium abundances were calculated for the measured aqueous H_2 concentrations in the final sample at each temperature condition. The dashed-dot lines indicate the concentration of CH_3OH required for thermodynamic equilibrium with the measured concentrations of ΣCO_2 and H_2 in the final sample of each stage of the experiment.

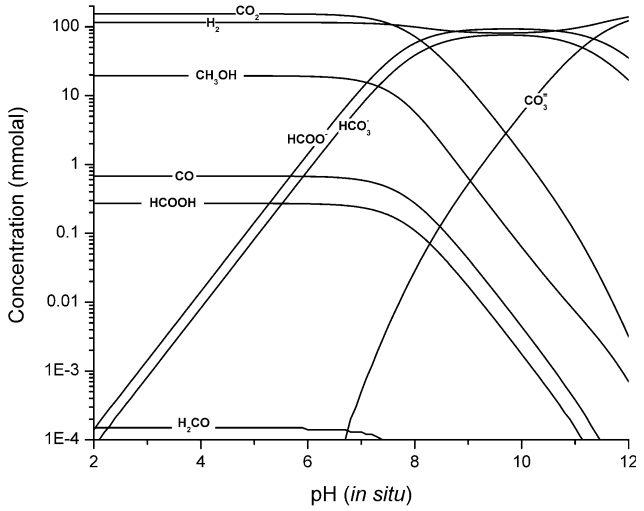

Fig. 4. Variation in the abundance of aqueous species as a function of pH at 300 °C and 350 bar in a solution initially containing 175 mmolal total C and H_2. Dissolved CH_4 was not considered in the chemical model due to kinetic barriers that prevent its formation on the time scale of laboratory experiments. Activity coefficients for all aqueous species were assumed to be unity. Requisite thermodynamic data for the construction of this figure are from the compilation of Johnson et al. (1992) and Shock (1995).

water–gas shift reaction had attained a state of thermodynamic equilibrium in less than 48 h at 300 °C.

A temperature reduction to 200 °C at 266 h resulted in a substantial increase in the concentration of ΣHCOOH while the CO concentration decreased slightly (Fig. 3B). These variations are consistent with the minor temperature dependence of the equilibrium constant for reactions (2) and (3) (Fig. 2). Comparison of observed fluid composition with predicted values suggests that thermodynamic equilibrium was attained within 115 h of reaction at 200 °C (Fig. 3B). Injection of deionized H_2O at 385 h resulted in CO and ΣHCOOH concentrations that decreased to a greater extent than can be accounted for by simple dilution of the reaction cell contents and rapidly approached an equilibrium state within 118 h after H_2O injection (Fig. 3C). In this case, equilibrium according to reaction (1) was approached from the direction of excess CO, while during the first stage of the experiment at 300 °C, equilibrium was approached from the direction of insufficient CO. Taken together, these results demonstrate that the water–gas shift reaction attained reversible states of thermodynamic equilibrium on the time scale of a few days at 200 and 300 °C.

After 510 h of reaction, temperature was reduced to 150 °C. A small decrease in the abundance of CO and an increase in ΣHCOOH were observed in the first 71 h following the temperature change (Table 1), consistent with the thermodynamic predictions based on the temperature dependence for reactions (2) and (3). Injection of additional CO and water at 722 h yielded a dissolved CO concentration of approximately 172 mmol/kg. Chemical interactions following injection resulted in continuous production of H_2, ΣCO_2, and ΣHCOOH, and decreasing CO as the fluid composition moved toward, but did not achieve, an equilibrium state after 141 h (Fig. 3D). Rapid increases in reaction rates were observed after increasing temperature to 200 °C (Fig. 3D). In particular, ΣHCOOH initially increased to a maximum concentration of 14 mmol/kg at 885 h before decreasing with continued reaction. The transient peak in ΣHCOOH abundance is consistent with the initial hydration of CO to form formic acid as an intermediate species (reaction (3)) that is subsequently oxidized to CO_2 (reaction (2)). When analyzed after 312 h of reaction at 200 °C, the fluid had reached a composition consistent with thermodynamic equilibrium according to reactions (1)–(3) (Fig. 3D).

Injection of isotopically labeled sodium bicarbonate ($NaH^{13}CO_3$) at 1248 h resulted in large decreases in the concentrations of CO, ΣCO_2, and H_2, and production of ΣHCOOH. Fluid speciation calculations conducted using the EQ3NR computer program yield an estimated in situ pH value of 8.2 at 1674 h. Alkaline conditions favor the formation of formate ($HCOO^-$), bicarbonate (HCO_3^-), and carbonate (CO_3^{2-}) according to the reactions:

$$HCOOH = H^+ + HCOO^-, \quad (5)$$

$$CO_{2(aq)} + H_2O = HCO_3^- + H^+, \quad (6)$$

$$HCO_3^- = CO_3^{2-} + H^+, \quad (7)$$

which in turn decreases the equilibrium concentrations of CO, $CO_{2(aq)}$, and HCOOH (Fig. 4). Calculated activities of dissolved species in the 1674 h sample approached values consistent with an equilibrium state constrained by the measured H_2 concentration (Fig. 3E). Similar calculations indicate an in situ pH of 8.8 after increasing temperature to 300 °C at 1680 h, and attainment of thermodynamic equilibrium appeared to occur within 188 h at this temperature. Dissolved H_2 increased to 19 mmol/kg in the sample taken at 1867 h following the increase in temperature to 300 °C. The cause of this increase is unknown but may reflect oxidation of the titanium reaction cell closure piece in response to the increased temperature.

Injection of NaHCOO at 300 °C after 1868 h of reaction produced substantial increases in H_2, ΣCO_2, CO, and ΣHCOOH (Fig. 3F). Fluid speciation calculations indicate an in situ pH value of 8.7 and the abundances of dissolved carbon species reached levels consistent with thermodynamic equilibrium within a few hours after injection. Results of the experiment following injection of $NaH^{13}CO_3$ and NaHCOO demonstrate rapid attainment of reversible equilibrium according to reactions 1, 2, 3 and 5, 6, 7 at 200–300 °C.

3.2. Methanol formation

Both formation and decomposition of methanol were observed during the course of the experiment. Mass spectrometric analyses prior to injection of unlabeled CO at 721.5 h indicate that within the resolution of the analysis, methanol produced during this phase of the experiment is

composed entirely of labeled carbon (Fig. 5). Production of $^{13}CH_3OH$ provides unequivocal evidence that this methanol was produced by the reduction of labeled carbon species and was not derived from decomposition of background carbon sources. In general, methanol concentrations remained constant at 150 °C and for most of the 200 °C phases of the experiment despite thermodynamic drives for production or destruction of this compound. At 300 °C, however, reaction rates were sufficiently rapid to cause methanol concentrations to increase when levels were below values required for thermodynamic equilibrium, and decrease when levels were in excess (Figs. 3A and D–F). The abundance of methanol approached near equilibrium values following injections of $NaH^{13}CO_3$ and NaHCOO at 300 °C (Figs. 3E and F). A maximum methanol concentration of 2.0 mmol/kg was observed at 200 °C in the 1200 h sample (Table 1), and likely reflects enhanced formation rates in response to the high concentrations of formic acid during this phase of the experiment.

Formaldehyde concentrations remained below the detection limit of our analytical technique (0.01 mmol/kg) in all fluids sampled during the experiment. Despite its lack of observation, formation of methanol from formic acid may have involved a formaldehyde intermediary (see Fig. 1) since its occurrence in solution at levels controlled by thermodynamic equilibrium would be well below our detection limit (Fig. 4).

3.3. Methane formation

The formation of small amounts of CH_4 (Table 1) along with lesser amounts of C_2–C_6 hydrocarbons (data not shown) was observed during the experiment. Mass spectrometric analysis of the sample at 48 h revealed that a small amount of ^{13}C was incorporated in CH_4, but not the longer chain hydrocarbons. The presence of ^{12}C in CH_4 and C_{2+} hydrocarbons indicate pyrolysis of background carbon sources contributed some carbon species to solution during the experiment. Relatively low concentrations of CH_4 relative to other carbon species indicates that the background sources of carbon were not large and did not contribute significantly to other single-carbon compounds observed during the experiment.

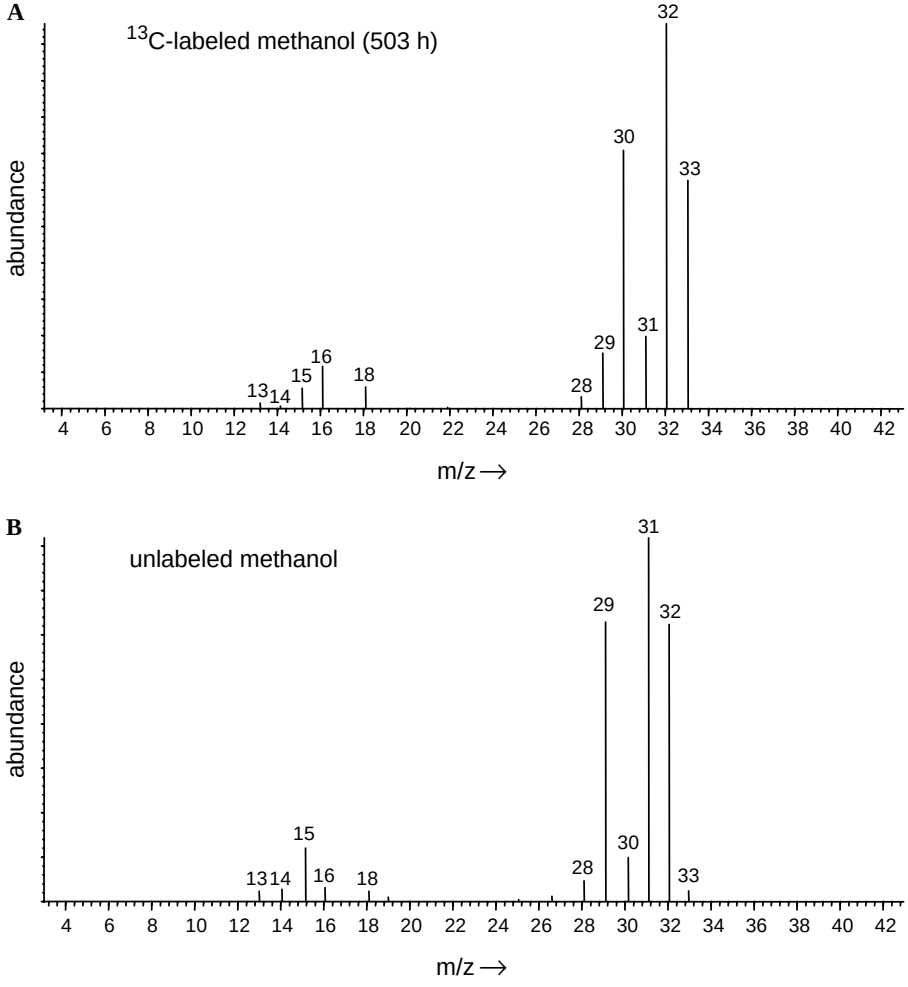

Fig. 5. Mass spectrum of (A) ^{13}C-labeled methanol in the 503 h fluid sample from the experiment and (B) a methanol standard containing natural abundances of carbon isotopes. Production of completely ^{13}C-labeled methanol at 503 h indicates formation via the reduction of labeled carbon species.

The presence of $^{13}CH_4$ at levels above natural abundances provides unequivocal evidence that some of the CH_4 was derived by reduction of labeled carbon species. Reduction of CO_2 to form CH_4 can be represented by the overall reaction

$$CO_2 + 4H_2 = CH_4 + H_2O \quad (8)$$

During all phases of the experiment, thermodynamic constraints favor this reaction to proceed to the right. However, stable equilibrium was not attained due to slow reaction kinetics for the formation of CH_4. This result is consistent with previous studies that have documented relatively sluggish reaction kinetics for the reduction of CO_2 to CH_4 under hydrothermal conditions in the absence of a catalyst (Berndt et al., 1996; Foustoukos and Seyfried, 2004; Horita and Berndt, 1999; McCollom and Seewald, 2001, 2003). Kinetic barriers that prevent the rapid formation of CH_4 allowed ΣCO_2, $\Sigma HCOOH$, and CO to persist at relatively high concentrations during the experiments and attain metastable equilibrium states according to reactions (1)–(3).

Temporal variations in the rate of CH_4 production can be used to elucidate the reaction path responsible for reduction of aqueous CO_2 to CH_4. Although relatively rapid CH_4 production might be expected during the 300 °C phases of the experiment due to the general positive correlation of increased reaction rates with the temperature, the fastest rate of CH_4 production was actually observed at 200 °C in the time period between increasing temperature at 863 h and the sample at 1175 h (Table 1). Although we did not determine the abundance of $^{13}CH_4$ during this phase of the experiment, the measured CH_4 concentration at 1175 h was substantially higher than the amounts observed from background sources at the start of the experiment (Table 1), suggesting that it was derived from CO_2 reduction. Methane production between 863 and 1175 h coincided with maximum methanol concentrations that approached 2 mmol/kg. The close association of CH_4 and methanol production suggests that the latter species may represent a reaction intermediary during the formation of CH_4 from CO_2. Collectively, these data suggest that formation of CH_4 from CO_2 during the experiments may not involve a heterogeneously catalyzed Fischer–Tropsch-type reaction, but instead may occur via an homogeneous, aqueous stepwise reduction path that produces $\Sigma HCOOH$, possibly formaldehyde, and methanol as reaction intermediaries according to the sequence shown in Fig. 1.

4. Discussion

4.1. Retrieval of kinetic data

Results of this study demonstrate that reactions involving ΣCO_2, $\Sigma HCOOH$, CO, and methanol occur at measurable rates at 150–300 °C on laboratory time scales and may attain metastable equilibrium states. During the experiment, the rate of CO disappearance is independent of thermodynamic drives when CO concentrations are far from equilibrium. A semi-log plot of far from equilibrium CO concentrations as a function of time reveals linear relationships (Fig. 6), suggesting that the rate of CO consumption is a first-order process with respect to CO abundance. Because oxidation of CO to CO_2 is a two-step process involving initial CO hydration (reaction (3)) followed by oxidation of formic acid to CO_2 (reaction (2)), the rate of CO disappearance can only be used to estimate the overall rate of CO oxidation if formic acid oxidation is substantially faster than the initial hydration step. The relatively minor transient peak in the abundance of formic acid at 885.5 h indicates that this is the case during CO oxidation at 200 °C (Table 1). Accordingly, the initial hydration of CO to formic acid appears to be the rate-limiting step during CO oxidation, and the rate of the overall water–gas shift reaction can therefore be represented by the expression

$$d[CO]/dt = k_{oxid}[CO], \quad (9)$$

where k_{oxid} is the rate constant for oxidation of CO to CO_2, [CO] is the concentration of aqueous CO, and t is time. Values of k_{oxid} at 150 and 200 °C were retrieved from the composition of fluids sampled at 737–861 h and 863–918 h, respectively. Linear regressions of log[CO] plotted against time yield rate constants of $3.51 \times 10^{-7}\ s^{-1}$ and $7.67 \times 10^{-6}\ s^{-1}$ at 150 and 200 °C, respectively. The temperature dependence of the rate constant can be described by the Arrhenius equation according to the relationship

$$\ln k_{oxid} = \ln A_o - E_a/RT, \quad (10)$$

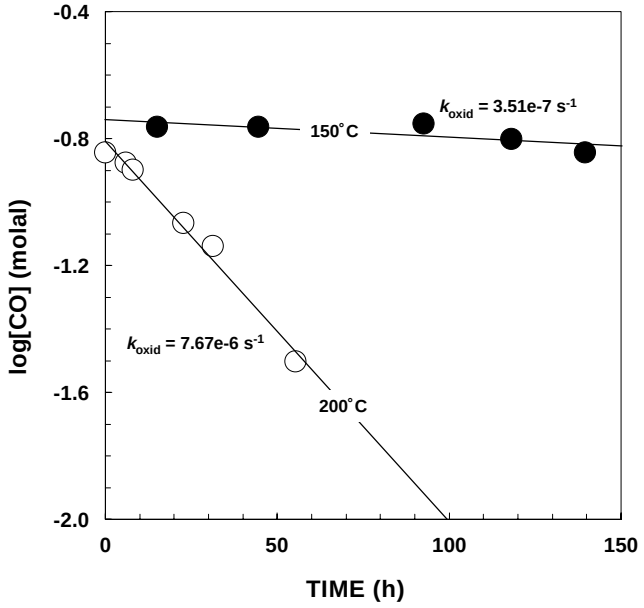

Fig. 6. Semi-log plot of far from equilibrium CO concentrations as a function of time during reaction of aqueous solutions at 150 and 200 °C. The linear relationships indicate that the decomposition of CO can be described by a first-order rate expression with respect to CO concentration.

where A_o is the preexponential factor, E_a is the activation energy, R is the ideal gas constant, and T is temperature in Kelvin. If it is assumed that reaction (3) is the rate limiting step during CO oxidation at temperatures $\gg$200 °C, then the results of our experiments can be compared with the data of Rice et al. (1998) who determined the rate of CO disappearance in supercritical water at 410, 450, and 480 °C over a wide range of water densities. These investigators demonstrated that for a given temperature the natural log of k_{oxid} varies linearly as a function of the natural log of water density. To assess the effect of temperature on the rate of CO oxidation at constant density, we extrapolated the rate data of Rice et al. (1998) to water densities during the experiments presented here. Ideally we would have also corrected the data from this study due to small differences in the density of water at 150 and 200 °C. This was not possible, however, because the dependence of k_{oxid} on water density at 150 and 200 °C is presently unknown. In the absence of such information, we opted to extrapolate the k_{oxid} values retrieved by Rice et al. (1998) to the average of water densities for the 150 °C (0.9354 g cm^{-3}) and 200 °C (0.8879 g cm^{-3}) phases of the experiment at 350 bar.

Examination of Fig. 7 reveals a linear temperature dependence for the value of $\ln k_{oxid}$ as a function of temperature from 150 to 480 °C that is consistent with Eq. (10). A linear regression of the collective data yields a preexponential factor of 1.35×10^6 s^{-1} and an activation energy of 102 kJ/mol. Some uncertainty is undoubtedly introduced to these values by our approximated water density for the 150 and 200 °C rate data. Although the amount of this error cannot be determined directly, separate regression of the rate constants determined here at 150 and 200 °C with Rice et al. (1998) values corrected for water densities at 150 and 200 °C, and 350 bar, indicates that values of E_a are affected by less than 2 kJ/mol, while values of A_o vary by less than an order of magnitude.

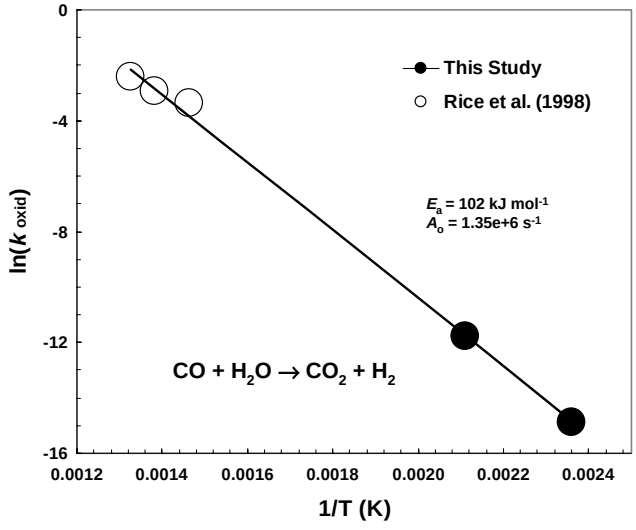

Fig. 7. Arrhenius plot of rate constants retrieved from the experimental data presented in this study and rate constants in supercritical water from Rice et al. (1998) for the water–gas shift reaction. A linear regression of the data yields an activation energy (E_a) of 102 kJ/mole and a preexponential factor (A_o) of 1.35×10^6.

4.2. Implications for seafloor hydrothermal systems

The abundance of CO, ΣHCOOH, and methanol in seafloor hydrothermal systems will be regulated by the residence time of fluids in reaction zones, and physical and chemical conditions in subsurface environments. A broad range of temperatures are associated with crustal circulation and seafloor venting of hydrothermal fluids. In ridge-crest systems, measured temperatures range from fluids marginally warmer than ambient 2 °C seawater to temperatures approaching the critical point of seawater at 407 °C (Von Damm, 1995). Variations observed for higher temperature fluids may reflect maximum subsurface conditions or varying degrees of cooling by subsurface mixing with cool seawater and/or conductive heat loss (Seewald et al., 2003; Seewald and Seyfried, 1990; Von Damm, 1995). In general, hydrothermal fluids in off-axis environments are characterized by lower temperatures. For example, the peridotite hosted Lost City vent field has a maximum measured temperature of 90 °C (Kelley et al., 2001, 2005) while vents issuing from the sediment covered flank of the Juan de Fuca Ridge have maximum recorded temperatures of 62 °C (Wheat et al., 2000).

Kinetic data retrieved for the water–gas shift reaction during this study can be used to evaluate the likelihood that concentrations of ΣCO_2, ΣHCOOH, and CO will evolve towards and perhaps attain a state of thermodynamic equilibrium at prevailing temperature, pH, redox conditions, and flow rates in subseafloor environments. At 350 °C, a typical temperature for black smoker vents, the calculated half-life for CO oxidation is of the order of 2 min, while at 100 °C, the reaction is characterized by a half-life of approximately 3 years (Fig. 8). Residence times for ridge-crest hydrothermal fluids are poorly constrained, but estimates for high temperature fluids (>200 °C) at various vent fields along the Juan de Fuca Ridge are $\leqslant$3 years (Kadko and Butterfield, 1998; Kadko and Moore, 1988). Minimum residence times at peak temperatures during circulation can be estimated from typical flow velocities and the depths to deep-seated reaction zones. If it is assumed that reaction zones are typically located at a depth of 1 km beneath the seafloor and fluid velocities of 2 m/s observed at the seafloor (Converse et al., 1984) extend to the reaction zone (i.e., pipe flow), then heated fluids must remain in the crust for a minimum of 500 s. In real systems, however, pipe flow in subsurface environments does not occur and fluids must accelerate as they are focused in vent structures during ascent. Moreover, the above calculation does not account for time spent at elevated temperatures during recharge. Thus, it is likely that the residence time of high-temperature ridge-crest hydrothermal fluids is substantially longer than the half-life for reaction (1), which is less than 16 min at temperatures of 300 °C and above. Con-

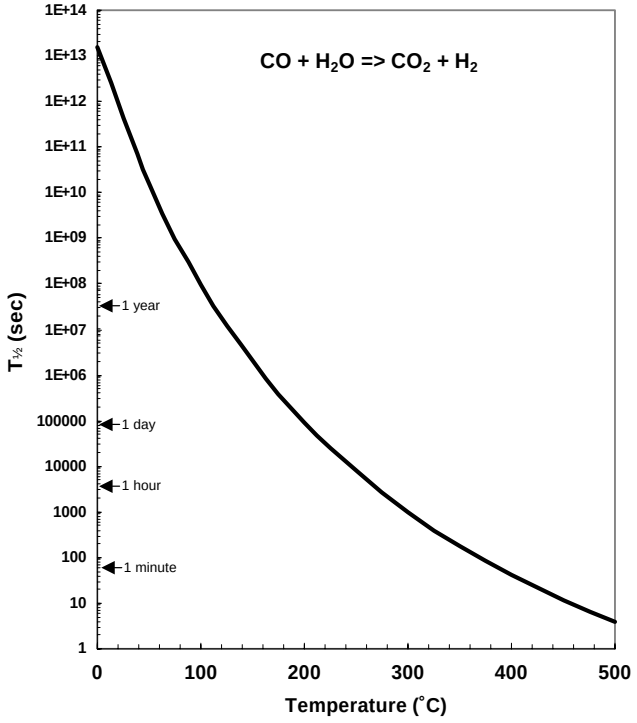

Fig. 8. Calculated half-life (s) for the oxidation of CO to CO_2 according to the water–gas shift reaction (reaction (1)).

sidering the relative magnitudes of the residence times and the rates for CO oxidation, it is highly likely that ΣCO_2, $\Sigma HCOOH$, and CO will attain a state of thermodynamic equilibrium in high temperature seafloor hydrothermal fluids.

Testing the hypothesis that the water–gas shift reaction reaches thermodynamic equilibrium in high temperature ridge crest hydrothermal systems requires quantitative data for the concentrations of CO_2, CO, and H_2 in vent fluids, as well as temperature and pH. Presently, requisite data are only available from the Rainbow vent field, Mid-Atlantic Ridge (Charlou et al., 2002), and the OBS and NGS vents at 21°N, East Pacific Rise (Lilley et al., 1983; Von Damm et al., 1985; Welhan and Craig, 1983). Redox conditions in these fluids are markedly different and reflect the variable composition of the oceanic crust in subsurface reaction zones. The Rainbow hydrothermal system is a peridotite-hosted system characterized by aqueous H_2 concentrations of 16 mmol/kg that result from serpentinization reactions (Berndt et al., 1996; McCollom and Seewald, 2001). In contrast, the 21°N system is hosted in basalt and H_2 concentrations at the OBS and NGS vents are significantly lower at 1.5 and 0.65 mmol/kg, respectively. To evaluate the extent of thermodynamic equilibrium according to the water–gas shift reaction at Rainbow and 21°N EPR, chemical affinities (A) were calculated according to the relationship

$$A = -RT \ln(Q/K_{eq}), \quad (11)$$

where R is the ideal gas constant, T is the temperature in Kelvin, Q is the activity product, and K_{eq} is the equilibrium constant. A positive chemical affinity indicates a thermodynamic drive for the reaction to proceed from left to right as written. Due to uncertainties in analytical and thermodynamic data, a value of zero is not expected for calculated affinities. For the purposes of this discussion, we consider calculated affinity values <5 kJ/mol as being consistent with a state of thermodynamic equilibrium. Although this value is somewhat arbitrary, it is similar in magnitude to uncertainties typically reported in the literature for thermodynamic data. Despite the substantial differences in fluid composition, chemical affinities for reaction (1) vary from 0.1 to 4.9 kJ/mol (Table 2). These values, which are close to zero, indicate dissolved CO_2 and CO concentrations in fluids at Rainbow and 21°N may have attained a state of thermodynamic equilibrium at the measured vent temperatures.

Rapid equilibration of the water–gas shift reaction during the experiments has substantial implications for understanding the potential for abiotic synthesis of organic compounds in hydrothermal systems. Theoretical models have shown that there is a strong thermodynamic drive for the formation of metastable aliphatic and aromatic hydrocarbons from CO_2 as submarine hydrothermal solutions are cooled below approximately 300 °C due to kinetic barriers that inhibit the formation of CH_4 and graphite (Shock, 1992; Zolotov and Shock, 1999). Zolotov and Shock (1999) point out that if kinetic barriers also prevent equilibration of CO with CO_2 and H_2 during cooling, quenching of elevated CO concentrations produced at high temperatures will result in a dramatic increase in the thermodynamic drive for abiotic organic synthesis from CO relative to synthesis from CO_2. From a mechanistic perspective, enhanced CO concentrations may also facilitate Fischer–Tropsch-type reactions. Results of the experiments presented here in conjunction with observations from natural hydrothermal systems, however, suggest that reaction of CO with CO_2 and H_2 is sufficiently rapid to maintain a state of thermodynamic equilibrium at temperatures

Table 2
Fluid chemistry and chemical affinities (A) for the water–gas shift reaction at Rainbow vent field, Mid-Atlantic Ridge, and OBS and NGS vents, 21°N East Pacific Rise

Location	Rainbow[a]	OBS[b]	NGS[b]
T(°C)	365	350	350
Depth (m)	2300	2500	2500
CO_2 (mmol/kg)	16	5.7	5.7
CO (nmol/kg)	5000	311	110
H_2 (mmol/kg)	16	1.5	0.65
CH_4 (mmol/kg)	2.5	0.06	0.07
$CO_{2(aq)} + H_{2(aq)} = CO_{(aq)} + H_2O_{(l)}$			
A_{250bar} (kJ/mol)	4.9	1.0	2.1
A_{500bar} (kJ/mol)	3.9	0.5	1.5
$A_{1000bar}$ (kJ/mol)	3.4	0.1	1.2

[a] Compositional data from Charlou et al. (2002).
[b] Compositional data from Lilley et al. (1983), Welhan and Craig (1983), Craig et al. (1980).

typical of most submarine hydrothermal systems. Accordingly, unless cooling of submarine hydrothermal fluids is extremely rapid, CO concentrations will reflect equilibration with CO_2 at the prevailing in situ fluid temperature and pressure, and thermodynamic drives for abiotic synthesis from CO and CO_2 will be similar.

Because reaction between CO_2 and CO in aqueous systems involves formation of a formic acid intermediate, equilibration of CO_2 and CO in vent fluids from the Rainbow and 21°N hydrothermal fields implies that ΣHCOOH should also be in equilibrium with these species. Compositional data do not exist for a similar assessment of the equilibrium state of methanol in hydrothermal fluids, but Voglesonger et al. (2001) proposed that synthesis of methanol occurs in axial hot-springs during diking events based on laboratory experiments that demonstrated magnetite-catalyzed production of methanol in a gas phase. Our results show that methanol formation occurs readily in an aqueous phase at 200–300 °C on laboratory time scales that are comparable to residence times for fluids in ridge-crest hydrothermal systems. Thus, methanol may be a ubiquitous component in CO_2-bearing vent fluids, even in the absence of a gas phase and magnetite.

To evaluate the likely speciation of carbon in subseafloor hydrothermal systems, concentrations of single carbon species were predicted as a function of temperature and fluid composition (Fig. 9). For the purpose of these calculations, thermodynamic equilibrium between ΣCO_2, CO, methanol, ΣHCOOH, and H_2 was assumed, while CH_4 was excluded from the equilibrium assemblage based on the experimental results and field observations that indicate kinetic barriers prevent its equilibration with other carbon species. Chemical conditions (ΣCO_2, H_2, and pH) were chosen to be representative of fluid compositions observed at many mid-ocean ridge vent systems (cf. Von Damm, 1995).

Examination of Fig. 9 reveals that lower temperatures and elevated H_2 activities favor the formation of reduced carbon compounds. Under high pH conditions, $HCOO^-$ is stabilized while the concentrations of CO_2, CO, and methanol decrease. These trends suggest that large variations in the abundance of single carbon compounds can be expected for the broad range of geochemical environments that characterize subseafloor hydrothermal systems. For example, the high temperature peridotite-hosted hydrothermal system at Rainbow that vents relatively low pH fluids containing 16 mmolal H_2 (Charlou et al., 2002) favors the formation of CO, formic acid, and methanol-rich fluids (Fig. 9B). Relatively high CO concentrations would suggest that Fischer–Tropsch synthesis of hydrocarbons may be likely in this environment. In contrast, low temperature and high pH at peridotite-hosted systems such as the Lost City hydrothermal field (Kelley et al., 2001, 2005) favor the formation of relatively minor CO (Fig. 9C). In reality, concentrations of aqueous carbon species at Lost City may be substantially lower than the values predicted in Fig. 9C because calcite solubility at the high pH of Lost City fluids will limit ΣCO_2 to very low abundances (Kelley et al., 2005). Accordingly, if CO represents a critical reactant for Fischer–Tropsch-type synthesis, then Lost City may not be the ideal environment for this type of reaction.

Relative to the more strongly reducing fluids like those at Rainbow and Lost City produced by reaction with peridotite, high-temperature basalt-hosted systems characterized by lower pH and H_2 concentrations are not expected to produce exceptionally high concentrations of ΣHCOOH and methanol, but should contain measurable CO (Fig. 9A). Significant amounts of reduced carbon compounds are expected, however, for conductively cooled high temperature basalt-hosted fluids (Fig. 9D), provided residence times are sufficiently long to accommodate reduced reaction rates at lower temperatures.

Cooling of high-temperature basalt-hosted fluids may also occur by mixing with cold seawater in subsurface environments. The effect of such mixing will be to enhance the relative stability of ΣHCOOH in response to lower temperatures and increased pH, but increased aqueous concentrations may not be realized due to dilution of the ΣCO_2-enriched hydrothermal fluid with relatively ΣCO_2-poor seawater. To model the chemical evolution of hydrothermal fluids during mixing of high temperature basalt-hosted vent fluids with relatively cool seawater, we conducted a reaction path calculation using the EQ3NR/EQ6 computer code (Wolery, 1992; Wolery and Daveler, 1992) and a thermodynamic database generated at 250 bar from the SUPCRT92 database (Johnson et al., 1992). The model used is analogous to that described in McCollom and Shock (1997) in which mixing starts with 1 kg of 350 °C hydrothermal fluid and incrementally adds 2 °C seawater. After each increment is added, an equilibrium composition and speciation of the fluid is calculated at the new temperature by minimizing the Gibbs free energy of the entire system. Because the present and prior studies have demonstrated kinetic barriers that prevent equilibration of CH_4 and more oxidized carbon species, reaction between CH_4 and all other carbon species was suppressed during these calculations. Similarly, equilibration between H_2S, SO_4, and intermediate oxidation state sulfur species was suppressed because previous studies have shown sluggish reaction rates (Ohmoto and Lasaga, 1982). Although reaction rates between aqueous H_2 in the hydrothermal fluid and O_2 in seawater are unknown, we opted to suppress reaction between these two species so that we could isolate the effects of equilibration amongst carbon species on measured H_2 concentrations. Retrieval of uncompromised H_2 concentrations from hydrothermal fluid samples that have undergone significant mixing with O_2-bearing seawater within fluid samplers (Seewald et al., 2002, 2003) suggests reaction between H_2 and O_2 may be sluggish. Quartz precipitation was suppressed in the model because quartz is rarely found in sulfide deposits formed by cooling of hydrothermal fluids and has been shown to behave conservatively during subsurface mixing (Von Damm and Lilley, 2004). The com-

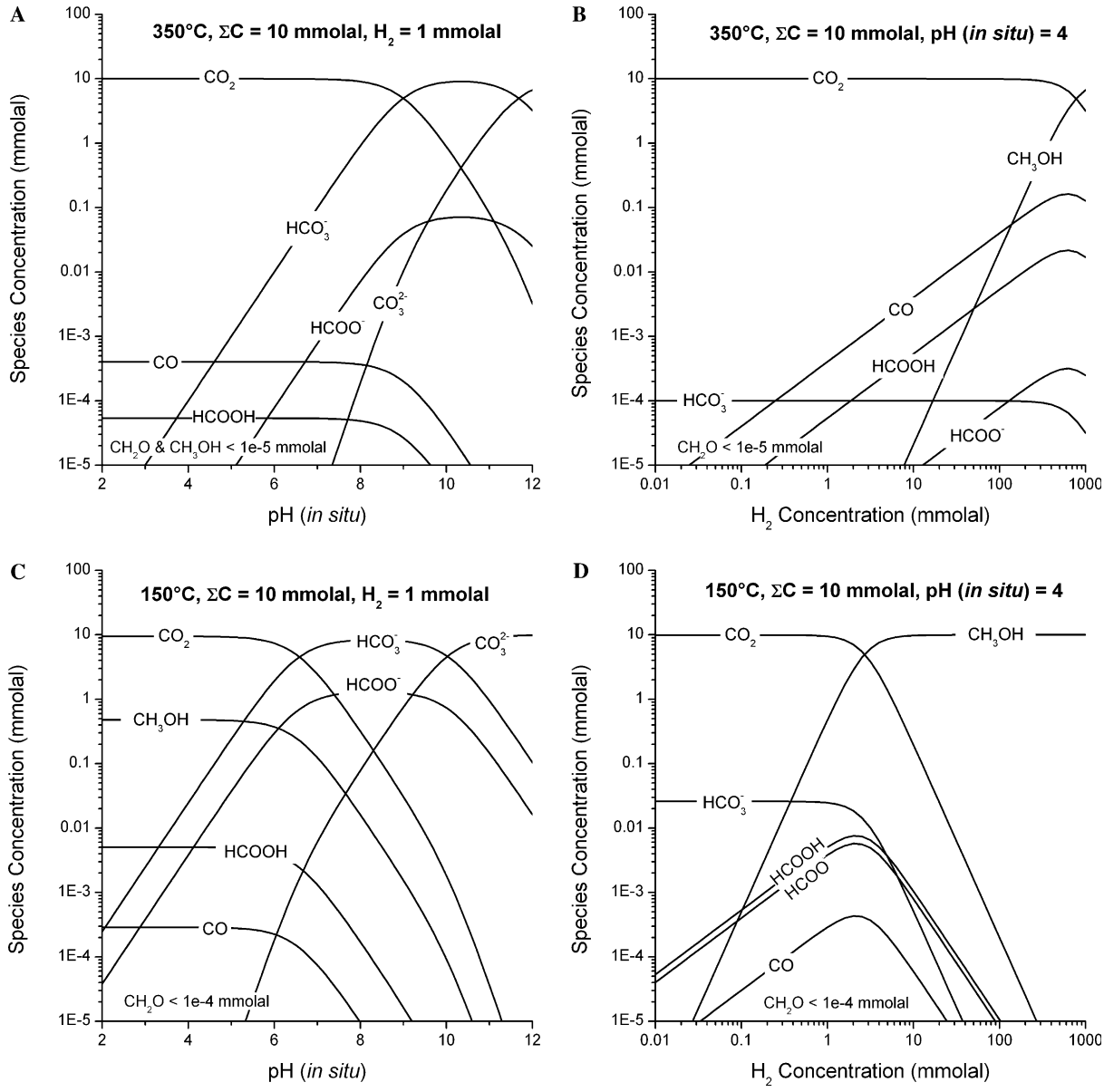

Fig. 9. Predicted concentrations of selected carbon species as a function of pH, (A and C), and H_2 concentration (B and D). A total carbon concentration of 10 mmolal was used in all plots. Dissolved CH_4 was not considered in the chemical model. Activity coefficients for all aqueous species were assumed to be unity. Requisite data for the construction of this figure are from the thermodynamic compilation of Johnson et al. (1992) and Shock (1995).

position of Bio9 and Bio9′ vents at 9°50′N EPR in November 1995 (Von Damm, 2004; Von Damm and Lilley, 2004) was used as the representative high temperature fluid in the model (Table 3). This location was chosen because diffuse fluids at 9 °50′N EPR vent field are well characterized and are in close proximity of focused flow high temperature vents (Von Damm, 2004; Von Damm and Lilley, 2004). Von Damm and Lilley (2004) have shown that diffuse fluids in this environment are produced by the subsurface mixing of seawater and nearby high temperature fluids.

Reaction path profiles for individual species indicate extensive reaction in response to changing temperature and chemical composition during mixing (Fig. 10). For example, CH_3OH and $HCOO^-$ increase dramatically with continued mixing, reaching μmolal concentrations in the low temperature fluids (Fig. 10). Aqueous HCOOH also increases with mixing but subsequently decreases due to increased pH that favors the formation of $HCOO^-$. The abundance of H_2 is predicted to increase during the initial stages of mixing due to pyrite precipitation, but subsequently decreases as CO_2 is reduced to form CH_3OH, $HCOO^-$, and HCOOH. Predicted decreases in the concentration of aqueous CH_4 are limited to the effect of dilution by CH_4-free seawater because reactions with other carbon species were suppressed in the model. Dissolved CO concentrations reach exceedingly low values in the low-temperature mixed fluid due to decreasing concentrations of H_2 and CO_2. These results demonstrate that mixing of a CO_2-rich high temperature fluid with cool seawater may represent an effective mechanism to generate significant

Table 3
Starting fluid compositions (mmol/kg) used for seawater–hydrothermal fluid mixing calculations

Species	Seawater	Hydrothermal fluid[a]
Na^+	468	391
K^+	10.2	14.5
Ca^{2+}	10.3	24
Mg^{2+}	52.3	0
Fe^{2+}	0	6.03
Cl^-	544	466
SO_4^{2-}	28.3	0
$SiO_{2(aq)}$	0.155	14.8
ΣH_2S	0	5.28
ΣCO_2	2.02	139
CH_4	0	0.084
H_2	0	0.36
pH (in situ)	8.2	4.5

[a] Hydrothermal fluid composition is from the Bio9 and Bio9′ vents at 9°50′, East Pacific Rise in November, 1995 (Von Damm, 2004; Von Damm and Lilley, 2004).

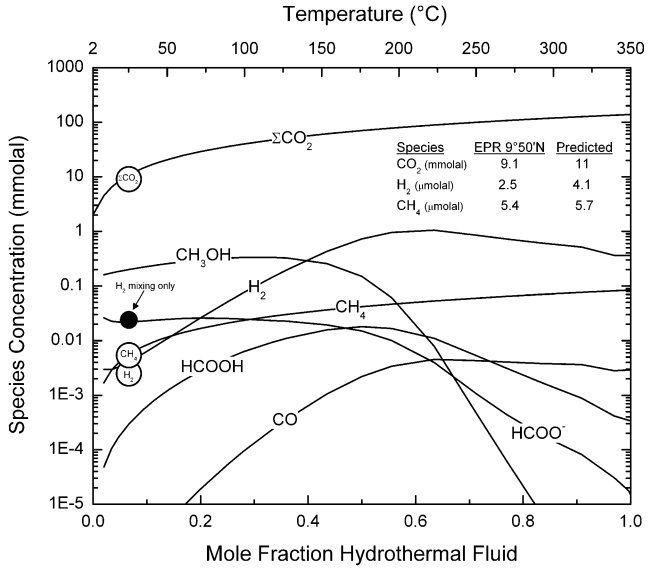

Fig. 10. Variations in the concentration of selected aqueous carbon species and H_2 predicted by a theoretical reaction path model during mixing of a 350 °C black-smoker hydrothermal fluid and 2 °C seawater (see text). The results are plotted against SiO_2 because it is a conservative tracer of mixing in hydrothermal fluids. The initial fluid compositions used for the model are shown in Table 3. The open circles represent observed concentrations of the indicated species in diffuse fluids from 9 °50′N EPR (Von Damm and Lilley, 2004). The solid circle represents the predicted concentration of H_2 in diffuse fluids 9°50′N EPR in the hypothetical case of conservative behavior during mixing.

quantities of methanol and ΣHCOOH in low-temperature vent fluids. Because vent ecosystems are limited to the relatively low temperature regions of seafloor hydrothermal systems, abiotic production of reduced carbon species in situ may influence metabolic strategies. Filamentous chemolithotrophic bacteria living in hot-springs at Yellowstone National Park, United States, for example, have been shown to metabolize formate despite the presence of abundant ΣCO_2 (Jahnke et al., 2001).

Comparisons of predicted fluid compositions for diffuse flow fluids at 9°50′N EPR reveal striking similarities. Indeed, a pervasive feature of the EPR fluids is aqueous H_2 concentrations that are approximately an order of magnitude lower than would be expected for conservative dilution during mixing (Von Damm and Lilley, 2004), indicating the presence of subsurface redox-dependent reactions. Similar trends have been reported for diffuse fluids at Axial Volcano on the Juan de Fuca Ridge (Butterfield et al., 2004). The measured H_2 concentration of 2.50 μmolal in diffuse fluids collected in November 1995 in the vicinity of the Bio9 and Bio9′ vents is reasonably consistent with the value of 3.96 μmolal predicted by the model (Fig. 10). The ability of the theoretical model to reproduce the composition of natural fluids suggests reduction of CO_2 to form methanol and ΣHCOOH may consume H_2 during mixing at 9°50′N EPR. Presently data for the abundance of methanol and ΣHCOOH are not available to test this hypothesis. The possibility that abiotic equilibration of carbon species may deplete hydrothermal fluids in aqueous H_2 concentrations has important implications for our understanding of microbial activity in a subsurface biosphere, since it removes H_2 as an easily metabolized energy source. Von Damm and Lilley (2004) have suggested that the large H_2depletions at 9°50′N EPR are attributable to microbial utilization of H_2 beneath the seafloor. The experimental and theoretical results presented here, however, suggest H_2 consumption during mixing may not be a unique feature of microbial activity.

5. Summary

Hydrothermal experiments demonstrate that reversible reactions between ΣCO_2, ΣHCOOH, CO, methanol, and H_2 in aqueous systems can be readily observed on a laboratory time scale at temperatures $\geqslant$150 °C without the addition of a heterogeneous catalyst. At temperatures $\geqslant$200 °C aqueous single carbon compounds may attain a state of redox dependent metastable equilibrium that does not include CH_4. Application of these results to submarine hydrothermal systems suggests that concentrations of single carbon compounds other than CH_4 may reach equilibrium states and vary systematically as a function of total C, the redox state of the fluid, and temperature. Thus, low-temperature basalt- and peridotite-hosted hydrothermal systems may generate reduced carbon compounds such as ΣHCOOH and methanol. Relatively low concentrations of CO predicted for low-temperature systems, however, suggest they may not be the optimum environment for abiotic synthesis of higher molecular weight reduced carbon compounds via Fischer–Tropsch-type processes. In contrast, peridotite-hosted systems characterized by high H_2 abundance and temperatures near 350 °C are expected to contain substantially higher CO concentrations that may enhance abiotic synthesis of longer chain hydrocarbons. The rather facile reaction between aqueous single carbon compounds at elevated temperatures suggests formation

of reduced single carbon compounds is a natural consequence of the strong thermal and chemical gradients that characterize subseafloor hydrothermal systems on Earth and other planetary bodies. Such processes may play a critical role in the maintenance of microbial populations in present-day vent ecosystems and the formation of organic precursors from which life evolved.

Acknowledgments

This study was supported by the National Science Foundation Grant #OCE-0136954, the Office of Basic Energy Sciences, U.S. Department of Energy Grant #DEF-G0297ER14746, and by NASA Exobiology Grant #NAG5-7696 and Origins Grant #NNG04GG23G. Helpful reviews by Mike Mottl and an anonymous reviewer are appreciated.

Associate editor: Jeffrey C. Alt

References

Anderson, R.B., 1984. *The Fischer–Tropsch Reaction*. Academic Press, London.

Bell, J.L.S., Palmer, D.A., 1994. Experimental studies of organic acid decomposition. In: Pittman, E.D., Lewan, M.D. (Eds.), *Organic Acids in Geological Processes*. Springer, Berlin, pp. 227–269.

Bell, J.S., Palmer, D.A., Barnes, H.L., Drummond, S.E., 1994. Thermal decomposition of acetate: III. Catalysis by mineral surfaces. *Geochim. Cosmochim. Acta* **58**, 4155–4177.

Berndt, M.E., Allen, D.E., Seyfried Jr., W.E., 1996. Reduction of CO_2 during serpentinization of olivine at 300 °C and 350 bar. *Geology* **24**, 351–354.

Burkhard, D.J.M., Ulmer, G.C., 1995. Kinetics and equilibria of redox systems at temperatures as low as 300 °C. *Geochim. Cosmochim. Acta* **59**, 1699–1715.

Butterfield, D.A., Roe, K.K., Lilley, M.D., Huber, J.A., Baross, J.A., Embley, R.W., Massoth G.J., **2004**. Mixing, reaction and microbial activity in the sub-seafloor revealed by temporal and spatial variation in diffuse flow vents at Axial Volcano. In: Wilcock, W.S.D., DeLong, E.F., Kelley, D.S., Baross, J.A., Cary, S.C. (Eds.), *The Subseafloor Biosphere at Mid-Ocean Ridges, AGU Monograph 144*. pp. 269–289.

Charlou, J.L., Donval, J.P., Fouquet, Y., Jean-Baptiste, P., Holm, N., 2002. Geochemistry of high H_2 and CH_4 vent fluids issuing from ultramafic rocks at the Rainbow hydrothermal field (36°14′N, MAR). *Chem. Geol.* **191** (4), 345–359.

Converse, D.R., Holland, H.D., Edmond, J.M., 1984. Flow rates in the axial hot springs of the East Pacific Rise (21°N): Implications for the heat budget and the formation of massive sulfide deposits. *Earth Planet. Sci. Lett.* **69** (1), 159–175.

Craig, H., Welhan, J.A., Kim, K., Poreda, R., Lupton, J.E., 1980. Geochemical studies of the 21°N EPR hydrothermal fluids. *EOS* **61** (45), 992.

Deines, P., Nafziger, R.H., Ulmer, G.C., Woermann, E., **1974**. T-fO_2 tables for selected gas mixtures in the C-H-O system. *College Earth and Mineral Sci. Bull. Exp. Station 88.* The Pennsylvania State Univ., University Park, PA.

Elliot, D.C., Sealock Jr., L.J., 1983. Aqueous catalyst systems for the water-gas shift reaction. 1. Comparative catalyst studies. *Ind. Eng. Chem. Prod. RD.* **22**, 426–431.

Foustoukos, D.I., Seyfried Jr., W.E., 2004. Hydrocarbons in hydrothermal vent fluids: the role of chromium-bearing catalysts. *Science* **304**, 1002–1005.

Horita, J., Berndt, M.E., 1999. Abiogenic methane formation and isotopic fractionation under hydrothermal conditions. *Science* **285**, 1055–1057.

Huebner, J.S., 1987. Use of gas mixtures at low pressure to specify oxygen and other fugacities of furnace atmospheres. In: Ulmer, G.C., Barnes, H.L. (Eds.), *Hydrothermal Experimental Techniques*. Wiley, New York, pp. 20–60.

Jahnke, L.L., Eder, W., Huber, R., Hope, J.M., Hinrichs, K.-U., Hayes, J.M., Des Marais, D.J., Cady, S.L., Summons, R.E., 2001. Signature lipids and stable carbon isotope analyses of Octopus Spring hyperthermophilic communities compared with those of *Aquificales* representatives. *Appl. Environ. Microbiol.* **67** (11), 5179–5189.

Johnson, J.W., Oelkers, E.H., Helgeson, H.C., 1992. SUPCRT92: a software package for calculating the standard molal thermodynamic properties of minerals, gases, aqueous species, and reactions from 1 to 5000 bar and 0 to 1000 °C. *Comput. Geosci.* **18**, 899–947.

Kadko, d., Butterfield, D.A., 1998. The relationship of hydrothermal fluid composition and crustal residence time to maturity of vent fluids on the Juan de Fuca Ridge. *Geochim. Cosmochim. Acta* **62**, 1521–1533.

Kadko, D., Moore, W., 1988. Radiochemical constraints on the crustal residence time of submarine hydrothermal fluids: Endeavour Ridge. *Geochim. Cosmochim. Acta* **52** (3), 659–668.

Kelley, D.S., Karson, J.A., Blackman, D.K., et al., 2001. An off-axis hydrothermal vent field near the Mid-Atlantic Ridge at 30° N. *Nature* **412**, 145–149.

Kelley, D.S., Karson, J.A., Früh-Geen, G.L., et al., 2005. A serpentine-hosted ecosystem: the Lost City hydrothermal field. *Science* **307**, 1428–1434.

Lilley, M.D., Baross, J.A., Gordon, L.I., 1983. Reduced gases and bacteria in hydrothermal fluids: the Galapagos spreading center and 21° N East Pacific Rise. In: Rona, P.E., Bostroem, K., Laubier, L., Smith, K.L., Jr.Jr. (Eds.), *Hydrothermal Processes at Seafloor Spreading Centers, NATO Conf. Ser. IV*. Plenum, New York, pp. 411–449.

McCollom, T.M., Seewald, J.S., 2001. A reassessment of the potential for reduction of dissolved CO_2 to hydrocarbons during serpentinization of olivine. *Geochim. Cosmochim. Acta* **65**, 3769–3778.

McCollom, T.M., Seewald, J.S., 2003. Experimental constraints on the hydrothermal reactivity of organic acids and acid anions: I. formic acid and formate. *Geochim. Cosmochim. Acta* **67**, 3625–3644.

McCollom, T.M., Shock, E.L., 1997. Geochemical constraints on chemolithoautotrophic metabolism by microorganisms in seafloor hydrothermal systems. *Geochim. Cosmochim. Acta* **61** (20), 4375–4391.

Melius C.F., N.E. Bergan, Shepherd J.E., **1991**. Effects of water on combustion kinetics at high pressure, *Proceedings of the 23rd Symposium (International) on Combustion*, Amer. Chem. Soc, pp. 217–223.

Ohmoto, H., Lasaga, A.C., 1982. Kinetics of reactions between aqueous sulfates and sulfides in hydrothermal systems. *Geochim. Cosmochim. Acta* **46** (10), 1727–1745.

Nafziger, R.H., Ulmer, G.C., Woermann, E., 1971. Gaseous buffering for control of oxygen fugacity at one atmosphere. In: Ulmer, G.C. (Ed.), *Research Techniques for High Pressure and High Temperature*. Springer, Berlin, pp. 9–41.

Rice, S.F., Steeper, R.R., Aiken, J.D., 1998. Water density effects on homogeneous water–gas shift reaction kinetics. *J. Phys. Chem. A* **102** (16), 2673–2678.

Seewald, J.S., Cruse, A., Saccocia, P.J., 2003. Aqueous volatiles in hydrothermal fluids from the Main Endeavour Field, northern Juan de Fuca ridge: temporal variability following earthquake activity. *Earth Planet. Sci. Lett.* **216**, 575–590.

Seewald, J.S., Doherty, K.W., Hammar, T.R., Liberatore, S.P., 2002. A new gas-tight isobaric sampler for hydrothermal fluids. *Deep-Sea Res.* **49**, 189–196.

Seewald, J.S., Seyfried Jr., W.E., 1990. The effect of temperature on heavy and base metal mobility in subseafloor hydrothermal systems: constraints from basalt alteration experiments and field studies. *Earth Planet. Sci. Lett.* **101**, 388B403.

Seyfried Jr., W.E., Janecky, D.R., Berndt, M.E., 1987. Rocking autoclaves for hydrothermal experiments, II. The flexible reaction-cell system. In:

Ulmer, Barnes, H.L. (Eds.), 1992, *Hydrothermal Experimental Techniques*. Wiley, New York, pp. 216–239.

Shock, E.L., 1992. Chemical environments of submarine hydrothermal systems; marine hydrothermal systems and the origin of life. *Origins Life Evol. Biosphere* **22** (1-4), 67–107.

Shock, E.L., 1995. Organic acids in hydrothermal solutions: standard molal thermodynamic properties of carboxylic acids and estimates of dissociation constants at high temperatures and pressures. *Am. J. Sci.* **295**, 496–580.

Ulmer, G.C., **1984**. ZrO_2 oxygen and hydrogen sensors: a geologic perspective. In: *Adv. Ceramics 12, Science and Technology of Zirconica II*, Amer. Ceram. Soc. pp. 660–671.

Voglesonger, K.M., Holloway, J.R., Dunn, E.E., Dalla-Betta, P.J., O'Day, P.A., 2001. Experimental abiotic synthesis of methanol in seafloor hydrothermal systems during diking events. *Chem. Geol.* **180** (1–4), 129–139.

Von Damm, K.L., 1995. Controls on the chemistry and temporal variability of seafloor hydrothermal fluids. In: Humphris, S., Zierenberg, R., Mullineaux, L., Thomson, R. (Eds.), *Seafloor Hydrothermal Systems: Physical, Chemical, Biological, and Geological Interactions*, AGU Monograph. 91, pp. 222–247.

Von Damm, K.L., 2004. Evolution of the Hydrothermal System at East Pacific Rise 9°50′N: Geochemical Evidence for Changes in the Upper Oceanic Crust. In: Christopher R. German, Jian Lin, Lindsay M. Parson (Eds.), *Mid-Ocean Ridges: Hydrothermal Interactions between the Lithosphere and Oceans*, Geophysical Monograph Series 148, pp. 285–304.

Von Damm, K.L., Edmond, J.M., Grant, B., et al., 1985. Chemistry of submarine hydrothermal solutions at 21°N, East Pacific Rise. *Geochim. Cosmochim. Acta* **49**, 2197–2220.

Von Damm, K.L., Lilley, M.D., 2004. Diffuse flow hydrothermal fluids from 9°50′N East Pacific Rise: Origin, evolution and biogeochemical controls. In: Wilcock, W.S.D., DeLong, E.F., Kelley, D.S., Baross, J.A., Cary, S.C. (Eds.), *The Subseafloor Biosphere at Mid-Ocean Ridges*, Geophyscial Monograph Series 144. pp. 245–268.

Welhan, J.A., Craig, H., 1983. Methane, hydrogen and helium in hydrothermal fluids at 21°N on the East Pacific Rise. In: Rona, P.E., Bostroem, K., Laubier, L., Smith, K.L., Jr.Jr. (Eds.), *Hydrothermal Processes at Seafloor Spreading Centers, NATO Conf. Ser. IV*. Plenum, New York, pp. 391–409.

Wheat, C.G., Elderfield, H., Mottl, M.J., Monnin, C., 2000. Chemical composition of basement fluids within an oceanic ridge flank: Implications for along-strike and across-strike hydrothermal circulation. *J. Geophys. Res.* **105** (B6), 13437.

Wolery, T.J., **1992**. EQ3NR, A Computer Program for Geochemical Aqueous Speciation-Solubility Calculations: Theoretical Manual, User's Guide, and Related Documentation (Version 7.0), Lawrence Livermore Nat'l. Lab.

Wolery, T.J., Daveler, S.A., **1992**. *EQ6, A Computer Program for Reaction Path Modeling of Aqueous Geochemical Systems: Theoretical Manual, User's Guide, and Related Documents*. Lawrence Livermore National Lab.

Zolotov, M., Shock, E.L., 1999. Abiotic synthesis of polycyclic aromatic hydrocarbons on Mars. *J. Geophys. Res.* **104** (E6), 14033–14049.